ACS OMEGA

Open Access

http://pubs.acs.org/journal/acsodf

Article

Theoretical Study of Gas Sensing toward Acetone by a Single-Atom Transition Metal (Sc, Ti, V, and Cr)-Doped InP_3 Monolayer

Xin Qin, Hao Cui, Lijuan Guo, Xin Li,* and Qiulan Zhou*

Cite This: *ACS Omega* 2024, 9, 45059−45067

Read Online

ACCESS | Metrics & More | Article Recommendations | Supporting Information

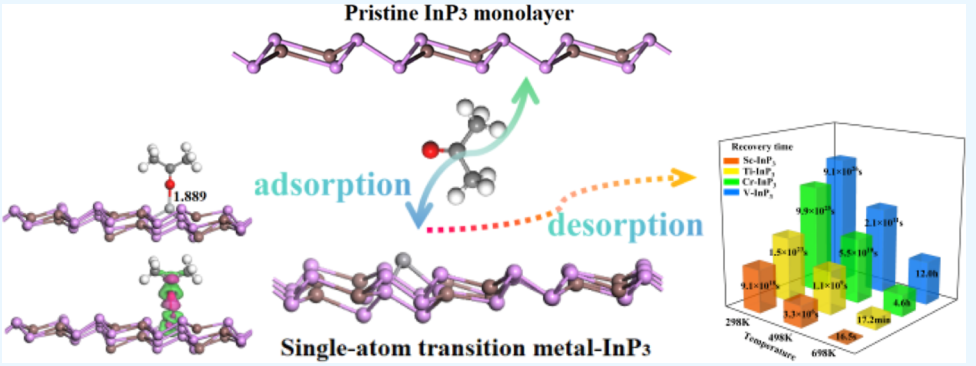

ABSTRACT: Acetone (C_3H_6O) gas in the exhaled breath of diabetic patients can be used as an important biomarker for the painless and noninvasive diagnosis of diabetes mellitus. In this paper, based on the density functional theory (DFT), the adsorption behaviors of pristine and single-atom transition metal (X = Sc, Ti, V, and Cr)-doped InP_3 surfaces (denoted as X-InP_3) toward C_3H_6O molecule were examined to explore the potential of these two-dimensional (2D) materials as a sensitive sensor for acetone gas. The calculation results indicate the unfavorable detection property for the pristine 2D-InP_3 surface upon acetone with an unsatisfied gas response (12.4%). The introduction of a single-atom transition metal (Sc, Ti, V, and Cr) into the InP_3 layer has significantly improved the adsorption capacity toward the C_3H_6O molecule. Owing to the high gas response values (−98.0%, 393.3%, and 393.3%), the Ti-InP_3, V-InP_3, and Cr-InP_3 layers show their superiority in C_3H_6O detection at room temperature, in which Ti-InP_3 achieves recycle use through heating at 698 K. Sc-InP_3 is unsuitable for C_3H_6O sensing with a poor response (8.1%). Our work first gives a theoretical predication about the adsorption and sensitive detection performance of pristine and single-atom transition metal (Sc, Ti, V, and Cr)-doped InP_3 upon acetone, which may provide an emerging kind of sensing material for the noninvasive diagnosis of diabetes mellitus indicated by acetone gas.

1. INTRODUCTION

Diabetes mellitus is a metabolic disease characterized by high fasting plasma glucose (HFPG), which causes many serious complications, such as coronary heart disease, stroke, and diabetic kidney disease.[1−3] Today, diabetes mellitus and its associated complications have become one of the leading causes of mortality worldwide.[4−6] The traditional method of diagnosing diabetes mellitus involves taking blood with a needle to measure glucose concentration, which many patients resist due to the discomfort of the needleprick.[7] Therefore, noninvasive diagnostic techniques for diabetes mellitus have attracted significant attention.[8−10] Acetone (C_3H_6O) is one of the volatile organic compounds (VOCs) found in human exhaled breath, and research has demonstrated that the concentration of acetone in the breath of diabetic patient is significantly higher compared to healthy individuals.[11−13] Consequently, respiratory C_3H_6O is considered as a potential biomarker for diabetes mellitus, and the detection of C_3H_6O gas for the noninvasive diagnosis of diabetes mellitus has garnered considerable concerned.[14,15]

Currently, detection methods in the field of breath analysis mainly include gas chromatography, mass spectrometry, electrochemical sensors, and spectroscopy.[16−19] Gas chromatography and mass spectrometry offer high sensitivity and specificity but are often limited by their complexity, high cost, and the need for skilled operators. Spectroscopy, including infrared and laser-based techniques, provides a noncontact method but may require expensive and sophisticated equipment. Among these methods, electrochemical sensors have

Received: June 10, 2024
Revised: October 19, 2024
Accepted: October 24, 2024
Published: October 30, 2024

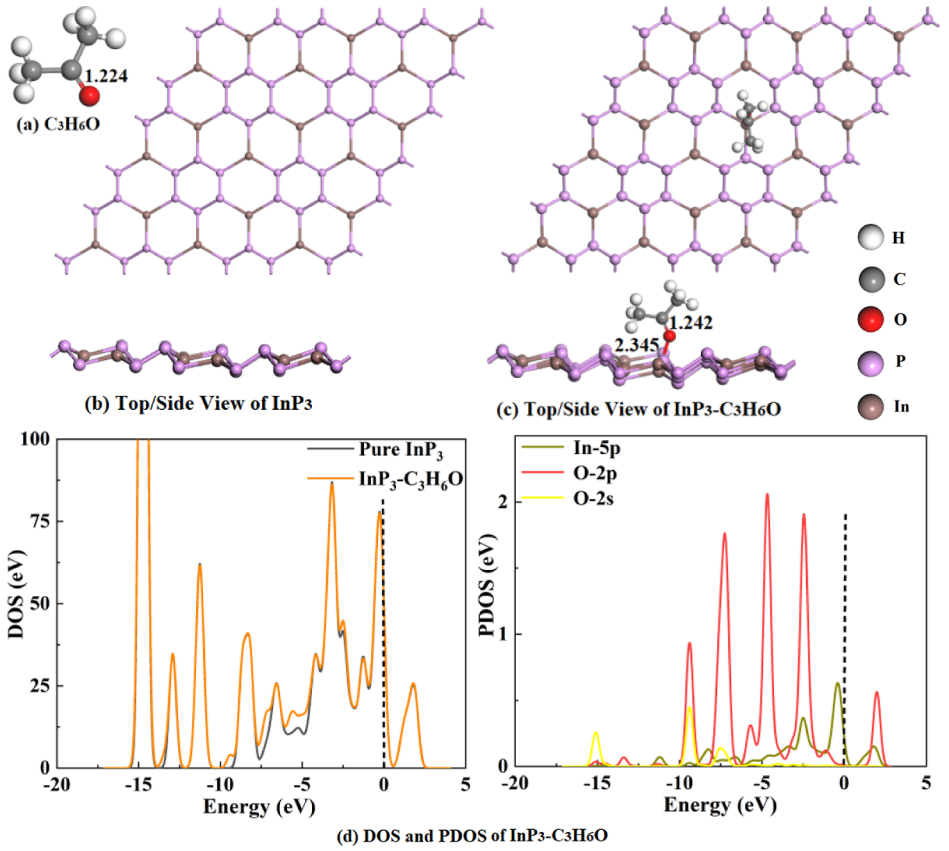

Figure 1. Optimized structures of C_3H_6O (a), 2D-InP_3 surface (b), InP_3-C_3H_6O adsorption system, (c) and DOS and PDOS of InP_3-C_3H_6O.

become the focus due to their advantages of small size, low cost, and simple manufacturing processes. These sensors typically operate by measuring changes in electrical properties, such as resistance or current, when C_3H_6O molecules interact with the sensor surface. The choice of a sensitive material is crucial for the sensing properties of gas sensors. As a result, a significant amount of research has been devoted to developing and optimizing these sensitive materials to improve the performance of C_3H_6O gas sensors.[20−22]

Owing to their large specific surface area, superior adsorption property, and fast response speed, two-dimensional (2D) materials have been widely studied for their acetone sensing capabilities.[23−25] For instance, an experimentally fabricated PbS nanosheet exhibit excellent acetone sensing with a response of 24.16% for 1 ppm concentration at room temperature.[26] Zhao and co-workers have demonstrated the good C_3H_6O sensing performance of synthetic $V_4C_3T_x$ MXene.[27] The prepared 2*D*/2D nanohybrid of the WO_3/WS_2 heterostructure by Yadav et al. showed an C_3H_6O response of 17.0% at a concentration of 1 ppm.[28] Additionally, theoretical studies have reported that the introduction of transition metal Pd can enhance the adsorption of BC_6N layer toward C_3H_6O gas.[29] Among all the 2D materials, the indium triphosphide (InP_3) monolayer has generated widespread attention due to its advantages in thermodynamical stability, adsorption capacities, and carrier mobility.[30,31] These properties make InP_3 an efficient nanomaterial in various application fields including energy storage, electronic devices, and gas sensors.[32−35] Miao and co-workers have theoretically demonstrated that monolayered InP_3 exhibits prominent excitonic effects and tunable magnetism, making it superior for electronic and photoelectric device.[36] Yi et al. have found that the δ-InP_3 material has high electron mobility and proposed it as a N-based gas sensor for NO_2 molecules.[37] Additionally, more unoccupied orbitals and lager atomic radius make transition metals ideal dopants, potentially leading to significant improvements in the electronic properties of nanomaterials through changes in chemical composition, band structure, and charge distribution.[38,39] Therefore, doping with transition metals is a highly effective method to regulate the physicochemical property of 2D materials. Ongoing research focuses on enhancing the performance of these materials through doping to optimize their chemical activity of the base material and improve the gas adsorption capacity.[40−42] Theoretical study by Liao et al. has shown that monatomic Cr-doped InP_3 could effectively enhance the adsorption toward H_2, C_2H_2 and CH_4.[43] Hou and co-workers have proven that the doping of transition metal (Mo, Fe, Pd, and Pt) could increase the adsorption capacity of InP_3 for SO_2 gas and has great application prospect as an SO_2 resistive sensor.[44] Although many previous studies show that InP_3 exhibits favorable gas sensing properties, the application of pristine and transition metal-doped InP_3 as an acetone sensor is still limited. Exploring InP_3 for acetone sensing is highly desirable for noninvasive diagnosis of diabetes mellitus. Computational predictions of InP_3-based materials for acetone sensing are a feasible and effective approach to promoting rapid development in this field.[35]

In this work, we put forward the hypothesis that the 2D-InP_3 and transition metal-modified InP_3 can be base materials for the adsorption and detection of acetone gas. To verify our assumption, the pristine 2D-InP_3 and four single-atom

https://doi.org/10.1021/acsomega.4c05405
ACS Omega 2024, 9, 45059−45067

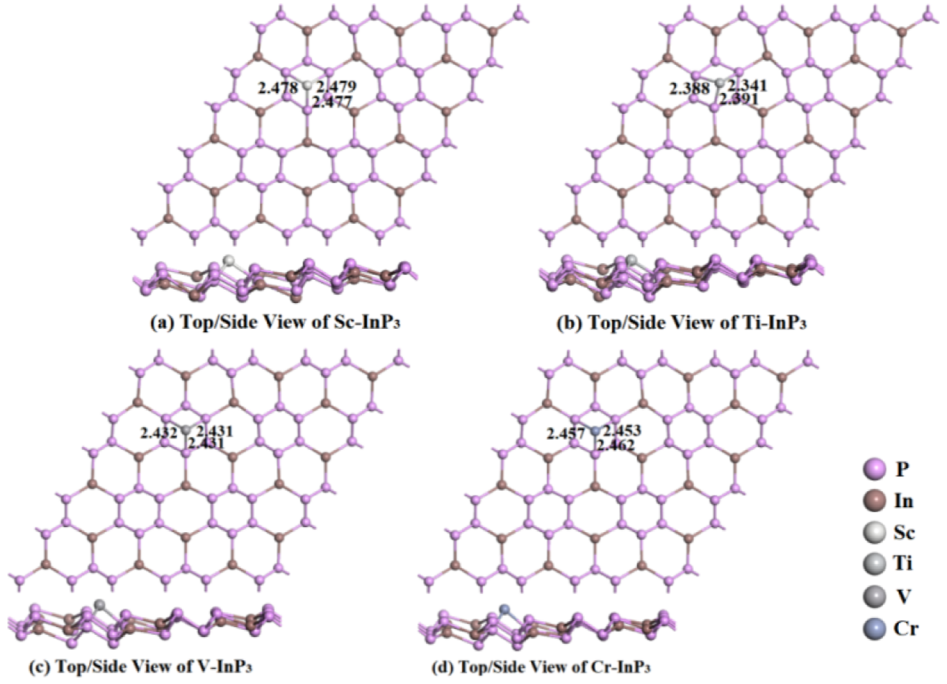

Figure 2. (a−d) Top and side views of the most stable Sc-InP_3, Ti-InP_3, V-InP_3, and Cr-InP_3. The distance is in Å.

transition metal (X = Sc, Ti, V, and Cr)-doped InP_3 monolayers (denoted as X-InP_3) were constructed. The adsorption behaviors of the pristine 2D-InP_3 and modified X-InP_3 (X = Sc, Ti, V, and Cr) surfaces toward the C_3H_6O molecule were investigated by density functional theory (DFT). The adsorption parameters, density of states (DOS), electron density difference (EDD), total charge density (TCD), and frontier molecular orbital (FMO) were discussed to compare the adsorption capability of these InP_3-based materials. The electrical conductivity, sensitivity response, and recovery time were analyzed to evaluate the applicability for acetone sensing. The calculation results show the potential application of a single-atom transition metal-doped InP_3 material in the noninvasive diagnosis of diabetes mellitus characterized by C_3H_6O gas.

2. RESULTS AND DISCUSSION

We first examined the adsorption behavior of pristine 2D-InP_3 toward C_3H_6O gas. The optimized structures of the C_3H_6O, 2D-InP_3 nanosheet, and InP_3-C_3H_6O adsorption system are shown in Figure 1. The lattice constant of the pristine 2D-InP_3 is 7.522 Å, and the bond lengths of In−P and P−P are 2.555 and 2.248 Å, which is consistent with the previous data.[45,46] The calculated frequency values (from 8.32 to 990.13 cm^{-1}) demonstrate the good stability of the 2D-InP_3 monolayer. In the InP_3-C_3H_6O system, the C_3H_6O molecule bonds to an In atom of InP_3 through its O atom with an In−O bond length of 2.345 Å. The length of the O−C bond in C_3H_6O slightly increases from 1.224 Å in the isolated molecule to 1.242 Å in the adsorption system. The adsorption energy (E_{ad}) between InP_3 and C_3H_6O is calculated as −0.962 eV, indicating a stable adsorption process. According to the Hirshfeld analysis, the adsorbed C_3H_6O acting as an electron donor transfers 0.147 e to the InP_3 surface. This electron transfer causes a slight charge redistribution on the InP_3 surface, potentially altering its electrical properties. Meanwhile, the change in band gap caused by the adsorption of C_3H_6O can induces corresponding changes in the electronic conductivity of the 2D-InP_3 materials.[43] In this study, the band gap of pristine 2D-InP_3 is 1.100 eV, which is consistent with the reported values,[33,45] whereas the band gap is slightly lower than the value (1.307 eV) calculated with the HSE03 functional due to the difference of calculation accuracy.[47] After adsorption of C_3H_6O, the band gap value slightly increases to 1.106 eV, reflecting the decreased conductivity in the InP_3-C_3H_6O adsorption system. Additionally, in the InP_3-C_3H_6O system, density of state (DOS) analysis reveals that C_3H_6O adsorption induces a decline of the DOS peak near the Fermi level, suggesting reduced electrical conductivity of the InP_3 nanosheet (Figure 1). This electronic interaction is further supported by the orbital overlap of In-5p and O-2p, as shown in the partial density of states (PDOS), highlighting the role of orbital hybridization in the C_3H_6O adsorption mechanism.

Besides, the gas response value (S) is employed to explain the degree of sensitive detection of pristine 2D-InP_3 toward C_3H_6O. The S is calculated as $S = (\sigma_{af}^{-1} - \sigma_{be}^{-1})/\sigma_{be}^{-1}$, where σ_{af} and σ_{be} denote the conductivity value of the system before and after adsorption. The conductivity value (σ) is related to the band gap (B_g) of the modified system, and the two physical quantities satisfy the formula $\sigma = \lambda e^{(-B_g/2\kappa T)}$, in which κ and T represent the Boltzmann constant [8.318×10^{-3} kJ/(mol K)] and temperature (set as 298 K in this study).[35] In accordance with the information presented above, the calculated sensitivity response for the InP_3-C_3H_6O system is only 12.4%. Therefore, taking the unsatisfied gas response and the E_{ad} value into comprehensive consideration, it reveals that the pristine 2D-InP_3 surface is inadequate for the sensitive detection of acetone gas.

To improve the sensitive detection performance of InP_3 for the acetone gas, four single-atom transition metals (Sc, Ti, V, and Cr) are, respectively, doped on the 2D-InP_3 surface to construct the X-InP_3 (X = Sc, Ti, V, and Cr) monolayer. The adsorption and detection behaviors of the four X-InP_3 (X = Sc,

https://doi.org/10.1021/acsomega.4c05405
ACS Omega 2024, 9, 45059−45067

Ti, V, and Cr) monolayers toward acetone gas are concurrently investigated.

To obtain the most stable structures of the four modified surfaces, the doped metal atom was placed at the possible binding sites, including the top of the In/P atom and the center of two six-membered rings, with the initial distance between the metal atom and InP_3 surface being 3.0 Å. The optimized geometric configurations of X-InP_3 (X = Sc, Ti, V, and Cr) are displayed in Figure 2. The most stable X-InP_3 (X = Sc, Ti, V, and Cr) surface, with the maximum binding energy (E_b), shows that the monoatom tends to locate above the P-hexatomic ring of InP_3, forming three new chemical X-P (X = Sc, Ti, V, and Cr). The shortest X-P bond lengths for Sc-InP_3, Ti-InP_3, V-InP_3, and Cr-InP_3 are 2.477, 2.341, 2.431, and 2.453 Å, respectively, as listed in Table 1.

Table 1. Corresponding Parameters of the Four X-InP_3 (X = Sc, Ti, V, and Cr) Monolayers

doped models	E_b (eV)	Q_T (e)	D (Å)
Sc-InP_3	−4.338	0.420	2.477
Ti-InP_3	−4.809	0.287	2.341
V-InP_3	−4.843	0.197	2.431
Cr-InP_3	−4.768	0.245	2.453

The binding energy (E_b) of a single Sc atom to InP_3 is 4.338 eV, which is lower than that of the other three doping nanosheets, with individual E_b values of 4.809, 4.843, and 4.768 eV for Ti, V, and Cr, respectively. After doping on the InP_3 surface, the four metal atoms donate 0.420, 0.287, 0.197, and 0.245 e to the InP_3 substrate, respectively. Meanwhile, compared with the pristine 2D-InP_3 monolayer, the band gaps of the four X-InP_3 (X = Sc, Ti, V, and Cr) surfaces reduce from 1.100 to 0.037, 0.218, 0.138, and 0.215 eV, respectively (Figure 3). This reduction is attributed to the doping of single-atom

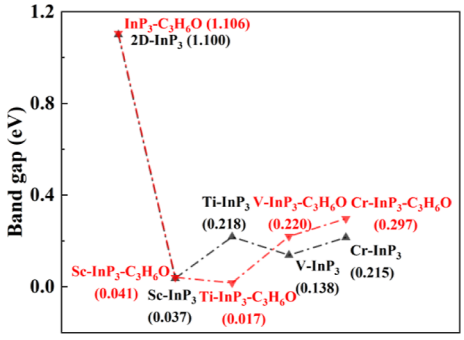

Figure 3. Trend chart of band gaps for the 2D-InP_3 and the four X-InP_3 (X = Sc, Ti, V, and Cr) monolayers (black dotted line) and for the InP_3-C_3H_6O and X-InP_3-C_3H_6O (X = Sc, Ti, V, and Cr) adsorption systems (red dotted line).

transition metals on the InP_3 surface, which promotes electronic interactions around the Fermi level. The decreased band gap reveals that the electronic conductivity of the four X-InP_3 (X = Sc, Ti, V, and Cr) materials accordingly increased. Figure 4 shows the DOS and PDOS of the four modified materials. The rise of DOS peaks near the Fermi level is related to the 3d electronic orbital of transition metal, synchronously indicating the enhanced electrical conductivity after metal atom doping on the InP_3 surface.[48] The DOS curves of the four X-InP_3 (X = Sc, Ti, V, and Cr) monolayers exhibit a significant left shift relative to the pristine 2D-InP_3 surface, which may be due to the sufficient orbital mixing between the P-3p orbit and the 3d orbit of the metal atom. Additionally, the DOS peaks of V-InP_3 and Cr-InP_3 systems near the Fermi level split into two small peaks compared to the pristine 2D-InP_3 monolayer.

Subsequently, the adsorption behaviors of the four X-InP_3 (X = Sc, Ti, V, and Cr) monolayers with respect to the C_3H_6O gas are analyzed. After geometry optimization, the most stable structures of C_3H_6O adsorbed on the four modified InP_3 surfaces along with the corresponding electron density difference (EDD) of the four adsorption systems are presented in Figure 5. The most stable structures show that the C_3H_6O molecule is positioned with its O atom oriented toward the transition metal dopant of the X-InP_3 (X = Sc, Ti, V, and Cr) substrate. The relevant lengths of the newly formed X-O (X = Sc, Ti, V, and Cr) bonds are 2.016, 1.889, 1.871, and 1.861 Å for Sc, Ti, V, and Cr, respectively. The shorter X-O (X = Sc, Ti, V, and Cr) bond distances in the four modified InP_3 systems indicate the enhanced adsorption performance between C_3H_6O and the X-InP_3 (X = Sc, Ti, V, and Cr) surfaces compared to that of the pristine 2D-InP_3 monolayer.

Table 2 provides the adsorption parameters of the four adsorption systems. The Sc-InP_3 surface shows weaker adsorption for the C_3H_6O molecule, with an E_{ad} of −1.831 eV, as indicated by the relatively long Sc−O bond length (2.016 Å). In contrast, the adsorption energies for the Ti-InP_3-C_3H_6O, V-InP_3-C_3H_6O, and Cr-InP_3-C_3H_6O systems are −2.080, −2.305, and −2.248 eV, respectively, revealing the enhanced adsorption capacity in comparison with the pristine 2D-InP_3 surface. These adsorption values of the modified InP_3 systems are comparable to that of the Ti-doped $MoSe_2$-C_3H_6O system,[48] which has an E_{ad} of −2.42 eV. In addition, the ZnO−O and the (110) face of SnO_2 are theoretically and experimentally proven to be effective sensing materials for C_3H_6O gas, with the corresponding E_{ad} being −1.06 and −1.63 eV,[49,50] which are obviously lower than the E_{ad} of the four X-InP_3 (X = Sc, Ti, V, and Cr) adsorption systems. Therefore, the modified InP_3 monolayer with single-atom transition metal doping exhibits superior adsorption properties for acetone gas, with the adsorption capacity in the order of V-InP_3 > Cr-InP_3 > Ti-InP_3 > Sc-InP_3.

Based on the Hirshfeld analysis, the C_3H_6O molecule carries positive charges of 0.171, 0.163, 0.101, and 0.100 e after adsorption on the Sc-InP_3, Ti-InP_3, V-InP_3, and Cr-InP_3 monolayers, respectively. The amount of charge transferred in Sc-InP_3-C_3H_6O and Ti-InP_3-C_3H_6O systems is larger than that in the pristine InP_3-C_3H_6O system, which indicates that the adsorption of C_3H_6O promotes the charge redistribution of Sc-InP_3 and Ti-InP_3 surfaces. The EDD (Figure 5) shows a sequential and dense distribution of electrons on the formed X-O (X = Sc, Ti, V, and Cr) bond, indicating orbital hybridization between the binding atoms and reflecting the chemisorption between the four X-InP_3 (X = Sc, Ti, V, and Cr) substrates and the C_3H_6O molecule.

Additionally, the interaction between X-InP_3 (X = Sc, Ti, V, and Cr) surfaces and C_3H_6O molecule is analyzed using the highest occupied (HOMO) and the lowest unoccupied molecular orbitals (LUMO) of molecule orbital theory.[51] Figure 6 displays the distributions of the HOMO−LUMO orbitals of the four adsorption systems. Due to the formation of the chemical X-O (X = Sc, Ti, V, and Cr) bond upon C_3H_6O adsorption, the LUMO orbitals mainly focus on the X-

https://doi.org/10.1021/acsomega.4c05405
ACS Omega 2024, 9, 45059−45067

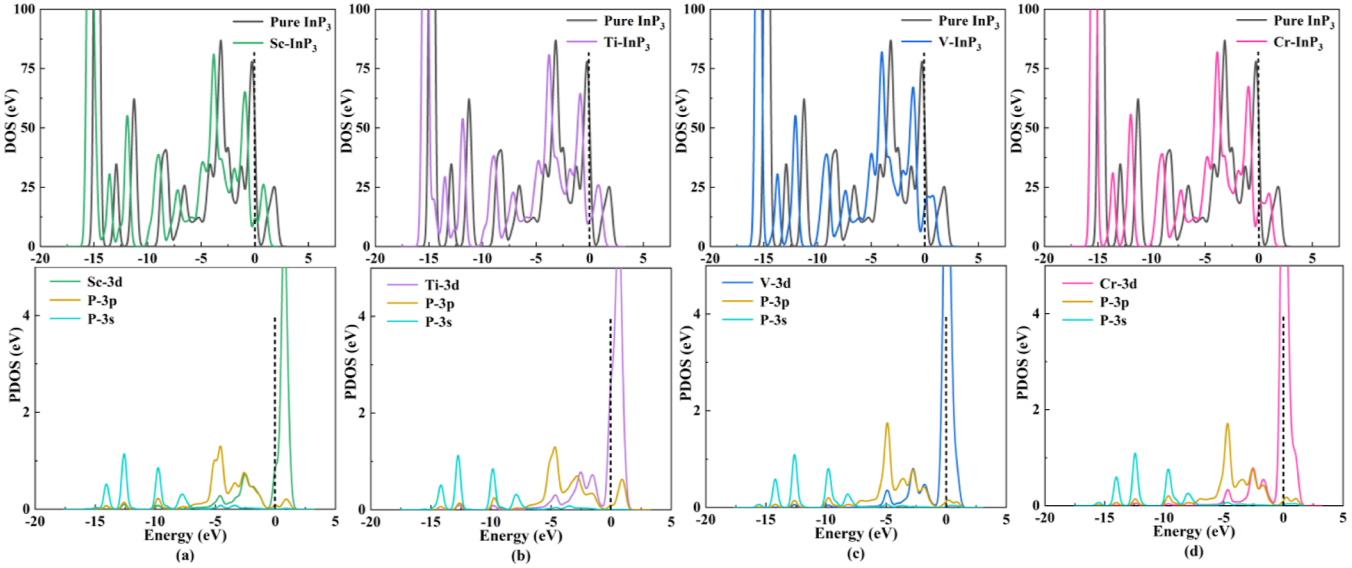

Figure 4. (a–d) DOS and PDOS of Sc-InP_3, Ti-InP_3, V-InP_3, and Cr-InP_3 systems. The dashed line is the Fermi level.

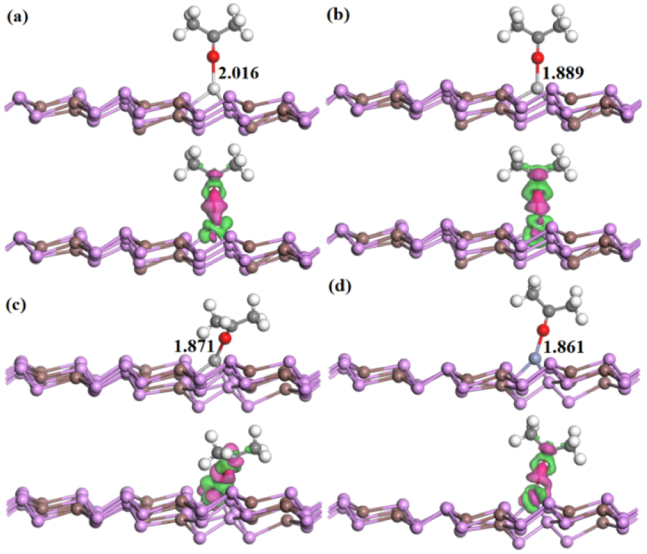

Figure 5. Most stable structures and EDD of the Sc-InP_3-C_3H_6O system (a), Ti-InP_3-C_3H_6O system (b), V-InP_3-C_3H_6O system (c), and Cr-InP_3-C_3H_6O system (d). The isosurface is 0.03 e/Å^3, and the distance is in Å.

Table 2. Adsorption Parameters and Gas Response Values of the X-InP_3-C_3H_6O (X = Sc, Ti, V, and Cr) Systems

adsorption systems	E_{ad} (eV)	Q_T (e)	D (Å)	S (%)
Sc-InP_3-C_3H_6O	−1.831	0.171	2.016	8.1
Ti-InP_3-C_3H_6O	−2.080	0.163	1.889	−98.0
V-InP_3-C_3H_6O	−2.305	0.101	1.871	393.3
Cr-InP_3-C_3H_6O	−2.248	0.100	1.861	393.3

O bond in the Sc-InP_3-C_3H_6O and V-InP_3-C_3H_6O systems, whereas in the Ti-InP_3-C_3H_6O and Cr-InP_3-C_3H_6O systems, the HOMO orbitals are abundant in the chemical X-O bonds. The difference in the energy gap (E_g) between HOMO and LUMO influences the conductivity of the adsorption system. The variation of E_g is defined as $(|E_g^{\text{X-InP}_3\text{-C}_3\text{H}_6\text{O}} - E_g^{\text{X-InP}_3}|)/E_g^{\text{X-InP}_3} \times 100\%$, in which $E_g^{\text{X-InP}_3}$ and $E_g^{\text{X-InP}_3\text{-C}_3\text{H}_6\text{O}}$ denote the energy gap of the four X-InP_3 (X = Sc, Ti, V, and Cr) surfaces before and after the adsorption of C_3H_6O. The calculated values for the four adsorption systems are 15.07%, 56.38%, 31.75%, and 16.44%, respectively. These results manifest that the order of change in conductivity for the four single-atom-modified InP_3 surfaces is Ti-InP_3 > V-InP_3 > Cr-InP_3 > Sc-InP_3.

The adsorption of the target molecule may have an impact on the distribution of band structure, leading to changes in the conductivity of the adsorption systems.[37] Therefore, we further analyzed the electrical conductivities of four X-InP_3 (X = Sc, Ti, V, and Cr) materials upon C_3H_6O adsorption. The density of states (DOS and PDOS) and total charge density (TCD) of the four adsorption systems are displayed in Figures 7 and 8. From the DOS curves, the decrease in the DOS peak at −2.0 and 1.0 eV in the Sc-InP_3-C_3H_6O system illustrates a reduction in electrical conductivity after the C_3H_6O adsorption, which is verified by the increase in the band gap from 0.037 eV in the Sc-InP_3 system to 0.041 eV in the Sc-InP_3-C_3H_6O adsorption system, as shown in Figure 3. For the Ti-InP_3-C_3H_6O system, the slight elevation of the DOS peak near the Fermi level conversely reveals an increase in the conductivity. Correspondingly, the band gap of the Ti-InP_3 system decreases from 0.218 to 0.017 eV after C_3H_6O adsorption, demonstrating an improvement in electrical conductivity. Furthermore, the V-InP_3-C_3H_6O and Cr-InP_3-C_3H_6O systems show a slight decline around −2.0 eV, indicating that C_3H_6O adsorption results in a minor reduction in the electrical conductivity. The band gaps of the V-InP_3 and Cr-InP_3 systems increase slightly from 0.138 and 0.215 eV to 0.220 and 0.297 eV after the adsorption of C_3H_6O (Figure 3), respectively, further indicating a decrease in conductivity of these adsorption systems.

From the PDOS curves, the emergence of the hybridization phenomenon between the 3d orbital of the transition metal atom and the O-2p orbital of C_3H_6O implies the formation of the X−O (X = Sc, Ti, V, and Cr) bonds, indicating the strong adsorption capacity of the X-InP_3 (X = Sc, Ti, V, and Cr) surface toward the C_3H_6O molecule. Besides, the PDOS curves show that 3d orbitals of transition metal atoms contribute more around the Fermi level in Ti-InP_3, V-InP_3, and Cr-InP_3

https://doi.org/10.1021/acsomega.4c05405
ACS Omega 2024, 9, 45059−45067

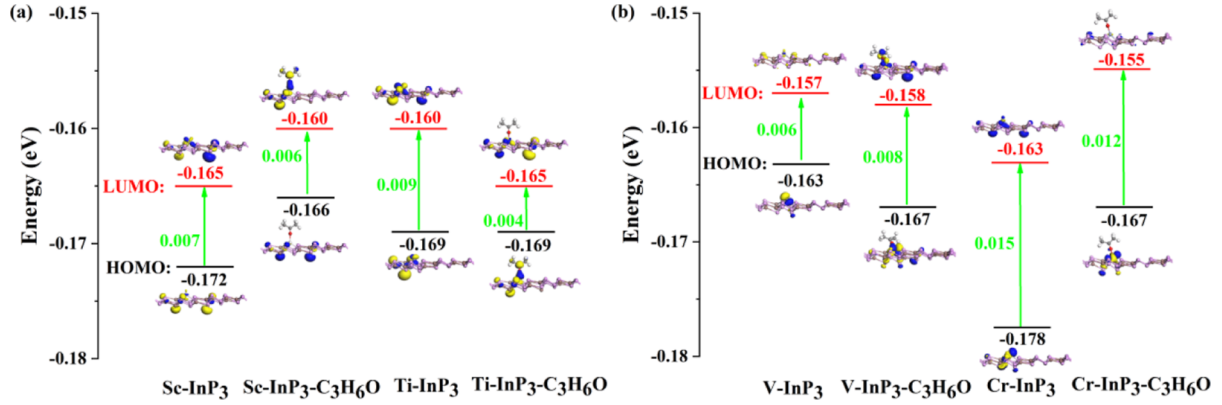

Figure 6. (a) HOMO and LUMO of Sc-InP_3 and Ti-InP_3 adsorption systems and (b) HOMO and LUMO of V-InP_3 and Cr-InP_3 adsorption systems.

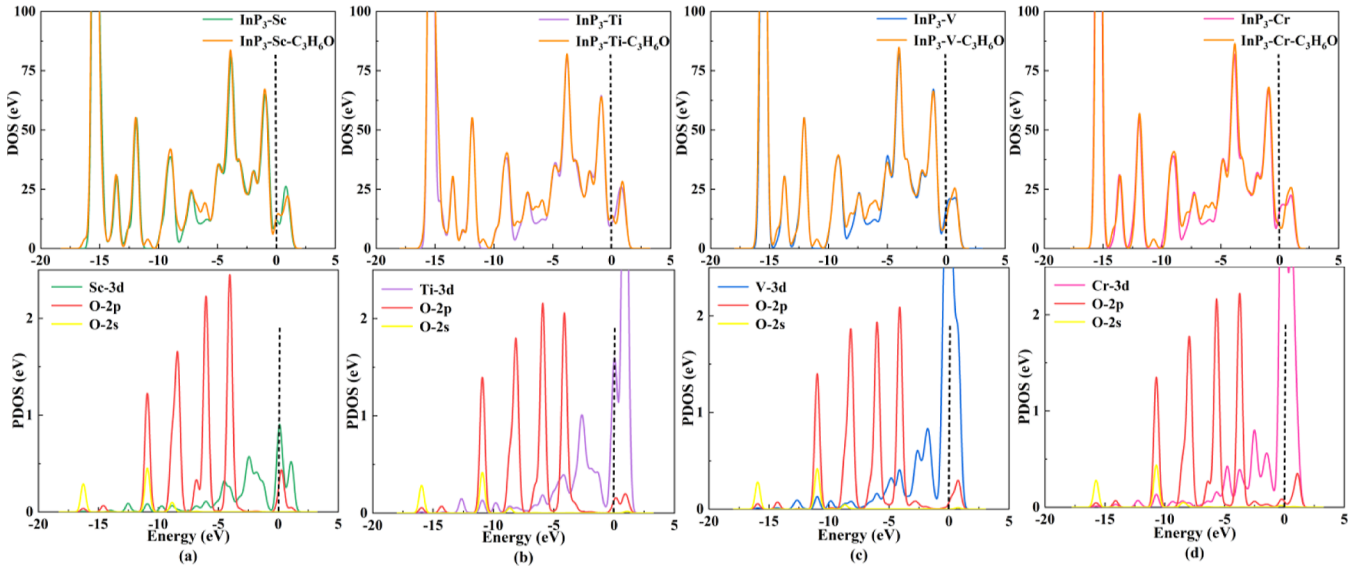

Figure 7. DOS and PDOS of Sc-InP_3-C_3H_6O system (a), Ti-InP_3-C_3H_6O system (b), V-InP_3-C_3H_6O system (c), and Cr-InP_3-C_3H_6O system (d). The dashed line is the Fermi level.

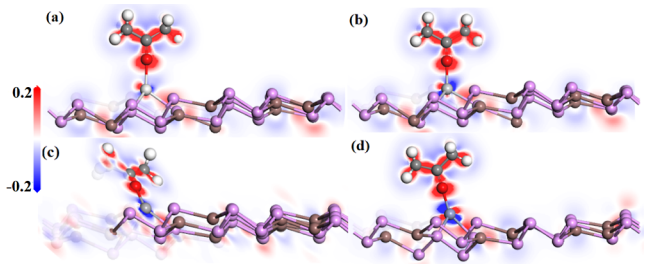

Figure 8. TCD of (a) Sc-InP_3-C_3H_6O, (b) Ti-InP_3-C_3H_6O, (c) V-InP_3-C_3H_6O, and (d) Cr-InP_3-C_3H_6O systems. The red/blue areas show electron accumulation/depletion.

adsorption systems. The TCD of the four adsorption systems shows that although electrons gather on the O atom of C_3H_6O due to its strong electronegativity, the C_3H_6O molecule is wholly surrounded by weak electron depletion. Additionally, the P atoms of the modified InP_3 surfaces show slight electron aggregation, which is consistent with the electron transfer obtained in the Hirshfeld analysis.

The suitability of 2D materials for gas sensing applications is better explored by gas-sensitive response in theoretical research. The gas-sensing responses of acetone on X-InP_3 (X = Sc, Ti, V, and Cr) monolayers were evaluated by the sensitivity response S, which is formulated as a combination of $S = (\sigma_{af}^{-1} - \sigma_{be}^{-1})/\sigma_{be}^{-1}$ and $\sigma = \lambda e^{(-B_g/2\kappa T)}$. The calculated S values for the Sc-InP_3-C_3H_6O, Ti-InP_3-C_3H_6O, V-InP_3-C_3H_6O, and Cr-InP_3-C_3H_6O systems are 8.1%, −98.0%, 393.3%, and 393.3%, respectively (Table 2). Compared to acetone sensors reported in previous works, The modified V-InP_3 and Cr-InP_3 surfaces achieve high sensitivity for C_3H_6O detection (Table S1), while the Ti-InP_3 exists an appropriate response upon C_3H_6O adsorption. The S value of Sc-InP_3-C_3H_6O is lower than that of the pristine 2D-InP_3 system, revealing a limited response for the Sc-InP_3 surface upon the C_3H_6O adsorption. To broaden the scope of application for the InP_3-based nanomaterials, the gas response values of 2D-InP_3 and X-InP_3 (X = Sc, Ti, V, and Cr) surfaces were investigated at operating temperatures ranging from 223 to 373 K. The results indicate that the acetone sensing responses of both 2D-InP_3 and X-InP_3 (X = Sc, Ti, V, and Cr) decrease as the temperatures increase (Table S2).

The desorption behaviors of C_3H_6O from the four X-InP_3 (X = Sc, Ti, V, and Cr) surfaces were estimated using the

https://doi.org/10.1021/acsomega.4c05405
ACS Omega 2024, 9, 45059−45067

recovery time (τ). τ is calculated with the van't Hoff-Arrhenius expression $\tau = A^{-1}e^{(-E_a/\kappa T)}$, in which A is the attempt frequency (10^{12} s^{-1}) and κ is the Boltzmann constant. E_a means the necessary energy for gas desorption, which is assumed as the numeric value of E_{ad} here.[52,53] The larger the E_{ad}, the higher the temperature required for gas desorption. Figure 9 shows the τ of X-InP_3 (X = Sc, Ti, V, and Cr) surfaces

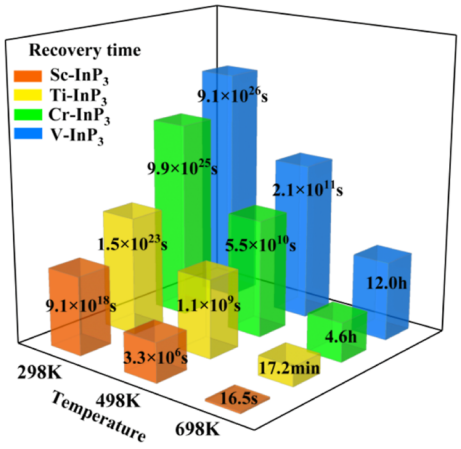

Figure 9. Recovery time of the four X-InP_3 (X = Sc, Ti, V, and Cr) monolayers for C_3H_6O desorption.

toward C_3H_6O at various temperatures. At ambient temperature, desorption of C_3H_6O from the four modified InP_3 materials is unrealistic, corroborating the chemisorption observed in the four adsorption systems. As the temperature increases, τ gradually decreases. Despite the long desorption time at 298 K, the calculated larger gas response values suggest that Ti-InP_3, Cr-InP_3, and V-InP_3 monolayers could be developed as high-performance sensing materials for C_3H_6O detection at room temperature. Meanwhile, Ti-InP_3 achieves its recycling in 17.2 min through heating at 698 K, which is an acceptable recovery time for the reusability of sensors.[54] Besides, the Sc-InP_3 surface, due to its low gas response, is unsuitable for C_3H_6O detection.

In summary, the calculated results in this study show the huge potentiality of a single-atom transition metal (Cr, V, and Ti)-doped InP_3 monolayer being the effective electrochemical devices for the sensitive detection of acetone gas. The theoretical research provides a novelty sensing material for the noninvasive diagnosis of diabetes mellitus utilizing the acetone markers. Additionally, beyond the parameters considered from a theoretical perspective, it is important to note that many practical factors and conditions may significantly impact the adsorption and sensitivity of modified InP_3 materials in detecting acetone gas. Therefore, extensive experimental research is necessary to explore its practical application value in the diagnosis of diabetes mellitus.

3. CONCLUSIONS

In this work, the adsorption behaviors of pristine 2D-InP_3 and single-atom transition metal (Sc, Ti, V, and Cr)-doped-InP_3 materials toward the C_3H_6O molecule were examined by employing the density functional theory. The analysis of the gas response value and adsorption parameters reveals that pristine 2D-InP_3 is inadequate for C_3H_6O detection. After single-atom transition metals (Sc, Ti, V, and Cr) are doped on the InP_3 monolayer, the enhanced adsorption energies and the distributions of frontier molecular orbitals demonstrate the chemisorption between the four X-InP_3 (X = Sc, Ti, V, and Cr) surfaces and C_3H_6O with the adsorption order being V-InP_3 > Cr-InP_3 > Ti-InP_3 > Sc-InP_3. The DOS curves and band gap values indicate the slight change of electrical conductivity in the four X-InP_3–C_3H_6O (X = Sc, Ti, V, and Cr) adsorption systems. The low response value (8.1%) shows that Sc-InP_3 is unsuitable for C_3H_6O sensing, while the high sensitivity responses (−98.0%, 393.3%, and 393.3%) allow Ti-InP_3, V-InP_3, and Cr-InP_3 surfaces becoming the potential sensing materials for C_3H_6O detection at room temperature. Ti-InP_3 realizes recycling through heating at 698 K. Therefore, the modified Ti-InP_3, V-InP_3, and Cr-InP_3 materials show promise for contributing to the noninvasive diagnosis of diabetes mellitus.

4. COMPUTATIONAL DETAILS

A 3 × 3 × 1 supercell of the primitive InP_3 monolayer and four single-atom transition metal (Sc, Ti, V, and Cr)-doped InP_3 surfaces with a vacuum space of 15 Å were established for the adsorption of acetone molecule.[47] All calculations were performed within the DMol[3] package on the basis of density functional theory (DFT).[55] The Perdew–Burke–Ernzerhof (PBE) with the generalized gradient approximation (GGA) was employed for the geometry optimizations and property calculations, in which the core and valence electrons were treated by the DFT semicore pseudopotentials (DSPPs) and the double numerical plus polarization (DNP).[56,57] The TS method for DFT-D was applied to better describe the van der Waals force and long-range interactions.[58] The Monkhorst–Pack k-point mesh of 3 × 3 × 1 and of 9 × 9 × 1 were adopt for geometric and electronic properties calculations with the global orbital cutoff radius being 5.0 Å. The energy tolerance accuracy, maximum force, and maximum displacement were 1 × 10^{-5} Ha, 2 × 10^{-3} Ha/Å, and 5 × 10^{-3} Å, respectively. Besides, the self-consistent field convergence accuracy was set as 1 × 10^{-6} Ha to ensure the high accuracy of the whole calculations.[47,59]

The binding energy (E_b) of single-atom transition metal (Sc, Ti, V, and Cr) on the InP_3 surface is calculated as $E_b = E_{X\text{-}InP_3} - E_{InP_3} - E_X$, where $E_{X\text{-}InP_3}$, E_{InP_3}, and E_x denote the total energy of the single-atom transition metal-doped InP_3 surface, the InP_3 monolayer, and the single-metal atom. The adsorption energy (E_{ad}) between pristine InP_3 and X-InP_3 (X = Sc, Ti, V, and Cr) surfaces with the C_3H_6O molecule is defined as $E_{ad} = E_{InP_3/C_3H_6O} - E_{InP_3} - E_{C_3H_6O}$, wherein E_{InP_3/C_3H_6O}, E_{InP_3}, and $E_{C_3H_6O}$ are the total energy for the InP_3 or X-InP_3 (X = Sc, Ti, V, and Cr) with the adsorbed C_3H_6O, the isolated InP_3 or X-InP_3 (X = Sc, Ti, V, and Cr) surface, and the C_3H_6O molecule, respectively. Generally, the adsorption system has a more negative E_{ad}, indicating the stronger interaction between the substrate and the target molecule.[35] The charge transfer (Q_T) between C_3H_6O and the InP_3 or X-InP_3 (X = Sc, Ti, V, and Cr) monolayer was quantitatively analyzed by the charge change of the adsorbed acetone on the basis of the Hirshfeld method, in which the negative Q_T value represents the adsorbed C_3H_6O as an electron acceptor, while the positive value denotes the bottom material as the electron acceptor.[60]

https://doi.org/10.1021/acsomega.4c05405
ACS Omega 2024, 9, 45059−45067

■ ASSOCIATED CONTENT

Supporting Information

The Supporting Information is available free of charge at https://pubs.acs.org/doi/10.1021/acsomega.4c05405.

Comparison of sensing responses for C_3H_6O and gas response values based on different temperatures (PDF)

■ AUTHOR INFORMATION

Corresponding Authors

Xin Li − *Hunan Provincial Key Laboratory of the Research and Development of Novel Pharmaceutical Preparations, "The 14th Five-Year Plan" Application Characteristic Discipline of Hunan Province (Pharmaceutical Science), College of Pharmacy, Changsha Medical University, Changsha 410219 Hunan, China*;
Email: tengyunxin2010@163.com

Qiulan Zhou − *Hunan Provincial Key Laboratory of the Traditional Chinese Medicine Agricultural Biogenomics, Hunan Provincial University Key Laboratory of the Fundamental and Clinical Research on Functional Nucleic Acid, "The 14th Five-Year Plan" Application Characteristic Discipline of Hunan Province (Clinical Medicine), Changsha Medical University, Changsha 410219 Hunan, China*;
Email: qlzhou@hnu.edu.cn

Authors

Xin Qin − *Hunan Provincial Key Laboratory of the Traditional Chinese Medicine Agricultural Biogenomics, Hunan Provincial University Key Laboratory of the Fundamental and Clinical Research on Functional Nucleic Acid, "The 14th Five-Year Plan" Application Characteristic Discipline of Hunan Province (Clinical Medicine), Changsha Medical University, Changsha 410219 Hunan, China*;
orcid.org/0000-0001-6275-4738

Hao Cui − *College of Artificial Intelligence, Southwest University, Chongqing 400715, Chongqing, China*;
orcid.org/0000-0002-9410-6345

Lijuan Guo − *School of Basic Medicine, Changsha Medical University, Changsha 410219 Hunan, China*

Complete contact information is available at: https://pubs.acs.org/10.1021/acsomega.4c05405

Notes

The authors declare no competing financial interest.

■ ACKNOWLEDGMENTS

This work was supported by the National Natural Science Foundation of China (No. 82203235), the Scientific Research Foundation of Hunan Provincial Education Department, China (Grant Nos. 23B0870, 23B0873, 22B0898, and 20A060), and Open Fund Project of Hunan Provincial Key Laboratory of the Research and Development of Novel Pharmaceutical Preparations (Grant No. 2023CYY007).

■ REFERENCES

(1) Su, M.; Hu, R.; Tang, T.; Tang, W.; Huang, C. Review of the correlation between Chinese medicine and intestinal microbiota on the efficacy of diabetes mellitus. *Front. Endocrinol.* **2023**, *13*, 1085092.

(2) Yu, T.; Xu, B.; Bao, M.; Gao, Y.; Zhang, Q.; Zhang, X.; Liu, R. Identification of potential biomarkers and pathways associated with carotid atherosclerotic plaques in type 2 diabetes mellitus: A transcriptomics study. *Front. Endocrinol.* **2022**, *13*, 981100.

(3) Liang, D.; Cai, X.; Guan, Q.; Ou, Y.; Zheng, X.; Lin, X. Burden of type 1 and type 2 diabetes and high fasting plasma glucose in Europe, 1990−2019: a comprehensive analysis from the global burden of disease study 2019. *Front. Endocrinol.* **2023**, *14*, 1307432.

(4) Fu, Q.; Chen, R.; Xu, S.; Ding, Y.; Huang, C.; He, B.; Jiang, T.; Zeng, B.; Bao, M.; Li, S. Assessment of potential risk factors associated with gestational diabetes mellitus: evidence from a Mendelian randomization study. *Front. Endocrinol.* **2024**, *14*, 1276836.

(5) Zhou, Y.; Chai, X.; Yang, G.; Sun, X.; Xing, Z. Changes in body mass index and waist circumference and heart failure in type 2 diabetes mellitus. *Front. Endocrinol.* **2023**, *14*, 1305839.

(6) Luo, M.; Cao, Q.; Wang, D.; Tan, R.; Shi, Y.; Chen, J.; Chen, R.; Tang, G.; Chen, L.; Mei, Z.; et al. The impact of diabetes on postoperative outcomes following spine surgery: A meta-analysis of 40 cohort studies with 2.9 million participants. *Int. J. Surg.* **2022**, *104*, 106789.

(7) Klonoff, D. C. Continuous glucose monitoring: roadmap for 21st century diabetes therapy. *Diabetes Care* **2005**, *28* (5), 1231−1239.

(8) Gudiño-Ochoa, A.; García-Rodríguez, J. A.; Ochoa-Ornelas, R.; Cuevas-Chávez, J. I.; Sánchez-Arias, D. A. Noninvasive Diabetes Detection through Human Breath Using TinyML-Powered E-Nose. *Sensors* **2024**, *24* (4), 1294.

(9) Pandey, R.; Paidi, S. K.; Valdez, T. A.; Zhang, C.; Spegazzini, N.; Dasari, R. R.; Barman, I. Noninvasive Monitoring of Blood Glucose with Raman Spectroscopy. *Acc. Chem. Res.* **2017**, *50* (2), 264−272.

(10) Zhang, Y.; Liu, Y.; Zhu, G.; Wang, Q.; Ni, J.; Liu, L.; Zhang, J.; Zhang, J.; Li, Z.; Wang, X.; et al. Noninvasive detection of diabetes mellitus based on skin fluorescence and diffuse reflectance spectroscopy. *J. Biophotonics* **2023**, *17* (1), No. e202300098.

(11) Rydosz, A. Micropreconcentrator in LTCC Technology with Mass Spectrometry for the Detection of Acetone in Healthy and Type-1 Diabetes Mellitus Patient Breath. *Metabolites* **2014**, *4* (4), 921−931.

(12) Pauling, L.; Robinson, A. B.; Teranishi, R.; Cary, P. Quantitative analysis of urine vapor and breath by gas-liquid partition chromatography. *Proc. Natl. Acad. Sci. U.S.A.* **1971**, *68* (10), 2374−2376.

(13) Henderson, M. J.; Karge, B. A.; Wren Shall, G. A. Acetone in the breath; a study of acetone exhalation in diabetic and nondiabetic human subjects. *Diabetes* **1952**, *1* (3), 188−193.

(14) Sun, M.; Chen, Z.; Gong, Z.; Zhao, X.; Jiang, C.; Yuan, Y.; Wang, Z.; Li, Y.; Wang, C. Determination of breath acetone in 149 type 2 diabetic patients using a ringdown breath-acetone analyzer. *Anal. Bioanal. Chem.* **2015**, *407* (6), 1641−1650.

(15) Wang, C.; Mbi, A.; Shepherd, M. A Study on Breath Acetone in Diabetic Patients Using a Cavity Ringdown Breath Analyzer: Exploring Correlations of Breath Acetone With Blood Glucose and Glycohemoglobin A1C. *IEEE Sens. J.* **2010**, *10* (1), 54−63.

(16) Schwoebel, H.; Schubert, R.; Sklorz, M.; Kischkel, S.; Zimmermann, R.; Schubert, J. K.; Miekisch, W. Phase-resolved real-time breath analysis during exercise by means of smart processing of PTR-MS data. *Anal. Bioanal. Chem.* **2011**, *401* (7), 2079−2091.

(17) Righettoni, M.; Tricoli, A.; Gass, S.; Schmid, A.; Amann, A.; Pratsinis, S. E. Breath acetone monitoring by portable Si:WO3 gas sensors. *Anal. Chim. Acta* **2012**, *738*, 69−75.

(18) Ghimenti, S.; Tabucchi, S.; Lomonaco, T.; Di Francesco, F.; Fuoco, R.; Onor, M.; Lenzi, S.; Trivella, M. G. Monitoring breath during oral glucose tolerance tests. *J. Breath Res.* **2013**, *7* (1), 017115.

(19) Sun, M.; Jiang, C.; Gong, Z.; Zhao, X.; Chen, Z.; Wang, Z.; Kang, M.; Li, Y.; Wang, C. A fully integrated standalone portable cavity ringdown breath acetone analyzer. *Rev. Sci. Instrum.* **2015**, *86* (9), 095003.

(20) Akhil, V. M.; Mangalore, S. J.; Chinmay, M. C.; Shankar, K. V.; Tawk, C. Effect of acetone treatment and copper oxide coating on the mechanical and wear properties of 3D-printed acrylonitrile butadiene styrene structures. *Virtual Phys. Prototyping* **2024**, *19* (1), No. e2345774.

(21) Cai, Z. Z.; Xu, C. X.; Song, Z. L.; Li, J. L.; Zhang, N.; Zhao, J. H.; Lee, Y. Y.; Reaney, M. J. T.; Huang, F. R.; Wang, Y. A two-step

method of cyclolinopeptide (linusorb) preparation from flaxseed cake via dry-screening. *Food Chem.* **2024**, *449*, 139243.
(22) Ji, X.; Chang, J.; Deng, Z.; Shen, C.; Li, M.; Wang, S.; You, L.; Kumar, M.; Fang, X.; Meng, G. Boosting acetone response of p-type Co3O4 sensor via Sn and Ni co-doping for diabetes diagnosis. *Sens. Actuators, B* **2024**, *410*, 135705.
(23) Chang, X.; Liu, X.; Zheng, W.; Zhou, L.; Zhang, J. Monolayer fullerene network: A promising material for VOCs sensor. *Appl. Surf. Sci.* **2023**, *637*, 157909.
(24) Raval, D.; Gupta, S. K.; Gajjar, P. N. Janus PdSTe nanosheet as promising contender for detection of volatile organic compounds (VOCs) in human breath: A first principles investigation. *Chem. Eng. J.* **2023**, *466*, 143101.
(25) Bhardwaj, R.; Hazra, A. SrTiO3 passivated MXene (Ti3C2Tx) for efficient VOC detection in hazardous humid ambient. *Sens. Actuators, B* **2024**, *401*, 134967.
(26) Jahromi, H. D.; Kazemi, M.; Sheikhi, M. H. Room temperature and highly sensitive acetone sensor based on lead sulfide nanosheets. *Mater. Sci. Eng., B* **2021**, *267*, 115082.
(27) Zhao, W. N.; Yun, N.; Dai, Z. H.; Li, Y. F. A high-performance trace level acetone sensor using an indispensable V(4)C(3)T (x) MXene. *RSC Adv.* **2020**, *10* (3), 1261−1270.
(28) Verma, A.; Yadav, B. C. 2D/2D Nanostructured System Based on WO3/WS2 for Acetone Sensor and Breath Analyzer. *ACS Appl. Nano Mater.* **2023**, *6* (7), 5493−5507.
(29) Jiang, X.; Luo, X. BC(6)N Monolayer as a Potential VOC Adsorbent in Mitigation of Environmental Pollution: A Theoretical Perspective. *ACS Omega* **2023**, *8* (49), 46841−46850.
(30) Ouyang, T.; Jiang, E.; Tang, C.; Li, J.; He, C.; Zhong, J. Thermal and thermoelectric properties of monolayer indium triphosphide (InP3): a first-principles study. *J. Mater. Chem. A* **2018**, *6* (43), 21532−21541.
(31) Sun, Z.; Yuan, K.; Chang, Z.; Bi, S.; Zhang, X.; Tang, D. Ultra-low thermal conductivity and high thermoelectric performance of two-dimensional triphosphides (InP(3), GaP(3), SbP(3) and SnP(3)): a comprehensive first-principles study. *Nanoscale* **2020**, *12* (5), 3330−3342.
(32) Chang, Y.; Wang, B.; Huo, Y.; Zhai, K.; Liu, L.; Li, P.; Nie, A.; Mu, C.; Xiang, J.; Zhao, Z.; et al. Layered porous materials indium triphosphide InP3 for high-performance flexible all-solid-state supercapacitors. *J. Power Sources* **2019**, *438*, 227010.
(33) Jalil, A.; Zhuo, Z.; Sun, Z.; Wu, F.; Wang, C.; Wu, X. A phosphorene-like InP3 monolayer: structure, stability, and catalytic properties toward the hydrogen evolution reaction. *J. Mater. Chem. A* **2020**, *8* (3), 1307−1314.
(34) Wu, W.; Zhang, Y.; Guo, Y.; Bai, J.; Zhang, C.; Chen, Z.; Liu, Y.; Xiao, B. Exploring anchoring performance of InP3 monolayer for lithium-sulfur batteries: A first-principles study. *Appl. Surf. Sci.* **2020**, *526*, 146717.
(35) Qin, X.; Luo, C.; Li, Y.; Cui, H. InP(3) Monolayer as a Promising 2D Sensing Material in SF(6) Insulation Devices. *ACS Omega* **2021**, *6* (44), 29752−29758.
(36) Miao, N.; Xu, B.; Bristowe, N. C.; Zhou, J.; Sun, Z. Tunable Magnetism and Extraordinary Sunlight Absorbance in Indium Triphosphide Monolayer. *J. Am. Chem. Soc.* **2017**, *139* (32), 11125−11131.
(37) Yi, W.; Chen, X.; Wang, Z.; Ding, Y.; Yang, B.; Liu, X. A novel two-dimensional δ-InP3 monolayer with high stability, tunable bandgap, high carrier mobility, and gas sensing of NO2. *J. Mater. Chem. C* **2019**, *7* (24), 7352−7359.
(38) Li, X.; Fu, Y.; Zhao, S.; Xiao, J.; Lan, M.; Wang, B.; Zhang, K.; Song, X.; Zeng, L. Metal ions-doped carbon dots: Synthesis, properties, and applications. *Chem. Eng. J.* **2022**, *430*, 133101.
(39) Danilovic, N.; Subbaraman, R.; Chang, K.-C.; Chang, S. H.; Kang, Y. J.; Snyder, J.; Paulikas, A. P.; Strmcnik, D.; Kim, Y.-T.; Myers, D.; Stamenkovic, V. R.; Markovic, N. M. Activity-Stability Trends for the Oxygen Evolution Reaction on Monometallic Oxides in Acidic Environments. *J. Phys. Chem. Lett.* **2014**, *5* (14), 2474−2478.
(40) Lu, Z.; Zhai, Y.; Liang, Q.; Wu, W. Promoting sensitivity and selectivity of NO2 gas sensor based on metal (Pt, Re, Ta)-doped monolayer WSe2: A DFT study. *Chem. Phys. Lett.* **2020**, *755*, 137737.
(41) Xie, T.; Wang, P.; Tian, C.; Zhao, G.; Jia, J.; Zhao, C.; Wu, H. The Adsorption Behavior of Gas Molecules on Co/N Co-Doped Graphene. *Molecules* **2021**, *26* (24), 7700.
(42) Zhang, M.; Guo, H.-m.; Lv, J.; Jia, J.-f.; Wu, H.-s. The 3d transition-metals doping tunes the electronic and magnetic properties of 2D monolayer InP3. *J. Magn. Magn. Mater.* **2021**, *533*, 168026.
(43) Liao, Y.; Zhou, Q.; Hou, W.; Li, J.; Zeng, W. Theoretical study of dissolved gas molecules in transformer oil adsorbed on intrinsic and Cr-doped InP3 monolayer. *Appl. Surf. Sci.* **2021**, *561*, 149816.
(44) Hou, T.; Zeng, W.; Zhou, Q. Adsorption Mechanism of SO2 on Transition Metal (Pd, Pt, Au, Fe, Co and Mo)-Modified InP3Monolayer. *Chemosensors* **2022**, *10* (7), 279.
(45) Li, Z.; Qian, M.; Song, L.; Ma, L.; Qiu, H.; Zeng, X. C. Tuning electronic structure of monolayer InP(3) in contact with graphene or Ni: effect of a buffer layer and intrinsic In and P-vacancy. *Phys. Chem. Chem. Phys.* **2019**, *21* (3), 1285−1293.
(46) Liu, J.; Liu, C.-S.; Ye, X.-J.; Yan, X.-H. Monolayer InP3 as a reversible anode material for ultrafast charging lithium- and sodium-ion batteries: a theoretical study. *J. Mater. Chem. A* **2018**, *6* (8), 3634−3641.
(47) Qin, X.; Cui, H.; Zhou, Q. Physisorption Behaviors of Organochlorine Pesticides on the InP(3) Monolayer from Theoretical Insight. *ACS Omega* **2023**, *8* (35), 32168−32175.
(48) Gao, C.; Liu, X.; Yang, H.; Zhou, Q.; Zhang, Y.; Yang, A.; Ye, H.; Liu, Y.; Zhang, L.; Zhang, G. A theoretical study of Ti−MoSe2 as a noninvasive type-1 diabetes diagnosis material for detecting acetone from exhaled breath. *Vacuum* **2020**, *182*, 109729.
(49) Du, H.; Yang, W.; Yi, W.; Sun, Y.; Yu, N.; Wang, J. Oxygen-Plasma-Assisted Enhanced Acetone-Sensing Properties of ZnO Nanofibers by Electrospinning. *ACS Appl. Mater. Interfaces* **2020**, *12* (20), 23084−23093.
(50) Chen, Y.; Qin, H.; Cao, Y.; Zhang, H.; Hu, J. Acetone Sensing Properties and Mechanism of SnO(2) Thick-Films. *Sensors* **2018**, *18* (10), 3425.
(51) Gui, Y.; Luo, P.; Ji, C.; Lin, Y.; Chen, X. First-Principles Study of the Gas Sensing of Benzene and Formaldehyde by Ag2O- and CuO-Modified MoSe2 Nanosheets. *ACS Appl. Nano Mater.* **2022**, *5* (9), 12907−12914.
(52) Chen, D.; Zhang, X.; Tang, J.; Cui, Z.; Cui, H. Pristine and Cu decorated hexagonal InN monolayer, a promising candidate to detect and scavenge SF(6) decompositions based on first-principle study. *J. Hazard. Mater.* **2019**, *363*, 346−357.
(53) Zhang, Y. H.; Chen, Y. B.; Zhou, K. G.; Liu, C. H.; Zeng, J.; Zhang, H. L.; Peng, Y. Improving gas sensing properties of graphene by introducing dopants and defects: a first-principles study. *Nanotechnology* **2009**, *20* (18), 185504.
(54) Rodrigues, D. C. M.; Amorim, R. G.; Latgé, A.; Venezuela, P. Improving the sensitivity of graphyne nanosensor by transition metal doping. *Carbon* **2023**, *212*, 118087.
(55) Delley, B. DFT studies: from molecules and molecular environments to surfaces and solids. *Comput. Mater. Sci.* **2000**, *17* (2−4), 122−126.
(56) Perdew, J. P.; Burke, K.; Ernzerhof, M. Generalized Gradient Approximation Made Simple. *Phys. Rev. Lett.* **1996**, *77* (18), 3865−3868.
(57) Delley, B. An all-electron numerical method for solving the local density functional for polyatomic molecules. *J. Chem. Phys.* **1990**, *92* (1), 508−517.
(58) Tkatchenko, A.; Scheffler, M. Accurate molecular van der Waals interactions from ground-state electron density and free-atom reference data. *Phys. Rev. Lett.* **2009**, *102* (7), 073005.
(59) Monkhorst, H. J.; Pack, J. D. Special points for Brillouin-zone integrations. *Phys. Rev. B* **1976**, *13* (12), 5188−5192.
(60) Hirshfeld, F. L. Bonded-atom fragments for describing molecular charge densities. *Theor. Chim. Acta* **1977**, *44* (2), 129−138.

https://doi.org/10.1021/acsomega.4c05405
ACS Omega 2024, 9, 45059−45067